



Search for a Fermiophobic Higgs Boson in the Di-photon Final State Using 7.0 fb^{-1} of CDF Data

The CDF Collaboration
URL <http://www-cdf.fnal.gov>
(Dated: May 17, 2011)

A search for a fermiophobic Higgs boson in the di-photon final states is reported based on CDF data from 7.0 fb^{-1} of integrated luminosity from $p\bar{p}$ collisions at $\sqrt{s}=1.96 \text{ TeV}$. In contrast with the Standard Model, the coupling of the Higgs boson to fermions is suppressed in fermiophobic models. Therefore, the diphoton decay mode can be greatly enhanced. In the presented note, no evidence of a resonance in the diphoton spectrum is observed, and upper limits are set on the cross section times branching fraction of the resonant state as a function of Higgs boson mass. We found an observed (expected) limit on the Fermiophobic Higgs boson production excluding Higgs bosons particles with a mass $m_{h,f} < 114 \text{ GeV}/c^2$ ($m_{h,f} < 111 \text{ GeV}/c^2$) at the 95% confidence level.

Preliminary Results

I. INTRODUCTION

The Standard Model (SM) prediction for $\gamma\gamma$ branching fraction is extremely small. However, in "fermiophobic" models, the coupling of the Higgs boson to fermions is suppressed. Thus, the decay of the Higgs boson to diphoton is greatly enhanced. In the SM, the spontaneously symmetry breaking mechanism requires a single doublet of a complex scalar field. However, nature does not have to follow this minimal version and that may require a multi-Higgs sector. Thus, extended Higgs sectors with doublets and triplets fields are in the market [1] [2]. We consider in this note a model that requires a doublet field. In this model, it is possible that the symmetry breaking mechanism responsible for giving masses to gauge bosons is separate from that which generates the fermion masses.

An informative summary of the various models that modify $B(h \rightarrow \gamma\gamma)$ can be found in Reference [3]. The "fermiophobic" Higgs (h_f) benchmark model assumes SM coupling to bosons and vanishing couplings to all fermions. In the case of h_f , gluon-fusion production vanishes and only associated production with a W or Z boson and vector boson fusion (VBF) remain. This results in a reduction in the production cross section by about a factor of four; however, this reduction is compensated by the branching fraction for these models, which can be larger by more than two orders of magnitude for low mass Higgs. For example, the branching fraction has as a value of one order of magnitude higher than those at SM for Higgs masses of about 120 GeV/ c^2 . The higher branching fraction causes a larger number of potential fermiophobic Higgs events compared to SM Higgs.

The diphoton final state is also appealing for a Higgs boson search because the photon ID efficiency and energy resolution are better than that of jets. The photons better energy resolution leads to a narrow M mass peak which can be exploited to reduce background.

In the past, there have been phenomenological discussions of searches for h_f at the Tevatron experiments [4], as well as experimental searches at LEP [5]. In Run I, CDF searched for the fermiophobic Higgs [6] and recently for Run II, DØ published a paper [7] focusing on the same search. Most recently, CDF published a search for h_f with $\sim 3 \text{ fb}^{-1}$ [8] and DØ published a search for the SM Higgs with $\sim 2.7 \text{ fb}^{-1}$ [9].

In this note, we will focus on the sensitivity of a CDF search for fermiophobic $H \rightarrow \gamma\gamma$. The first fermiophobic result in this channel by CDF was obtained using 3.0 fb^{-1} of data with central ($|\eta| < 1.1$) and "plug" ($1.2 < |\eta| < 2.8$) photons. The current result increases sensitivity by 55% with 7.0 fb^{-1} of data and the addition of two improvements: (a) reducing jet backgrounds for regular central photons using a neural network (NN) discriminator and (b) reconstructing central photons that convert into an electron-positron pair. The use of the latter improvements allows for two new channels to be added: a central-central conversion category (CC conversion) where a regular central photon and a central conversion photon are identified; and a central-plug conversion category (CP conversion) where one regular plug photon and a central conversion photon are found. The first improvement, using a NN to identify central photons, most significantly enhances the CC channel where two central photons are selected, but additionally benefits the CP and CC conversions categories which also include central photons.

All cross sections are calculated by HIGLU and branching fractions are calculated by HDECAY [10]. These values are summarized in Table I.

M_h (GeV/ c^2)	$\sigma(Wh)$ pb	$\sigma(Zh)$ pb	$\sigma(VBF)$ pb	$B(h_f \rightarrow \gamma\gamma)$
100	0.2919	0.1698	0.1001	0.182
105	0.2484	0.1459	0.0923	0.106
110	0.2120	0.1257	0.0851	0.062
115	0.1745	0.1039	0.0786	0.038
120	0.1501	0.0902	0.0727	0.028
125	0.1295	0.0785	0.0671	0.022
130	0.1120	0.0685	0.0621	0.019
135	0.0972	0.0600	0.0575	0.012
140	0.0846	0.0527	0.0532	0.006
145	0.0737	0.0463	0.0494	0.003
150	0.0644	0.0408	0.0458	0.002

TABLE I: Cross section for Fermiophobic Higgs production, and its branching fractions decay to diphotons for many mass points.

II. THE CDF DETECTOR

A detailed description of the CDF detector is described in many available references [11, 12].

III. DATA SETS AND GLOBAL EVENT SELECTION

This analysis uses data from February 2004 and June 2010 comprising approximately 7.0 fb^{-1} of integrated luminosity. Signal Monte Carlo (MC) was generated using PYTHIA 6.2 [13] using CTEQ5 [14] parton distribution functions, and the standard CDF underlying event tune [15]. Samples for masses between $100 - 150 \text{ GeV}/c^2$ in $5 \text{ GeV}/c^2$ intervals were generated and used.

The global event selection requires that the data was taken during good detector conditions, that the event vertex be within $|z_{vtx}| < 60 \text{ cm}$, that the two photons have transverse energy $E_T > 15 \text{ GeV}$, and that their invariant mass be greater than $30 \text{ GeV}/c^2$. This selection is exactly the same as the published high-mass search for Randall-Sundrum gravitons decaying to the $\gamma\gamma$ final state [16] and therefore will not be discussed in detail here. The only difference for this result is that a different trigger is used, which is described below.

In order to improve sensitivity, the event selection was further extended to take advantage of the final state features present in these production modes. Associated production dominates the production process, so the optimization was carried out on the basis of the associated production process alone. A selection based on the fact that fermiophobic Higgs events will be produced with Z or W bosons or two jets which will balance the high diphoton transverse momentum. We considered the cut of 75 GeV as in the previous analysis which is termed as the high p_T bin. Moreover, we added two more p_T bins, $35 \text{ GeV} < p_T < 75 \text{ GeV}$ (medium p_T bin) and a lower p_T bin $p_T < 35 \text{ GeV}$.

Recent diphoton analyses at CDF have used diphoton triggers [16, 17]. Photon conversions, however, are suppressed by these triggers due to a requirement that an electromagnetic (EM) cluster profile be consistent with that of an isolated single EM object. In order to increase acceptance for photon conversions, it was decided instead to use a high- p_T inclusive photon trigger which relaxes this requirement. This trigger additionally requires one cluster of electromagnetic energy to have $E_T > 25 \text{ GeV}$, the EM cluster can be loosely isolated, and that only a small fraction of the total E_T associated with the cluster be hadronic. It was found that this trigger in place of the diphoton triggers provides about the same acceptance in the regular photon channels, but greater acceptance in the conversion channels.

The inclusive photon trigger efficiency for our cuts in each channel was obtained using Higgs diphoton MC samples. For each photon in an event, simulated trigger variables were determined assuming trigger tower clustering and a $z_{vtx} = 0 \text{ cm}$. If at least one photon in the event passed all trigger selection, then the trigger efficiency for each channel was obtained by taking the ratio of the events that pass all diphoton selection and the trigger to those that pass the diphoton selection.

The resulting efficiencies applied for each test mass and channel are plotted in Figure 1. The trigger efficiencies for the CC channel are about 100%, as they were for the diphoton trigger used in previous diphoton analyses. For the CP channel they range from about 96-100% from lower to higher masses, for the CC conversion channel they range from 98-99% and for the CP conversion channel they range from 86-97%. The statistical binomial errors seen in the figure are applied as systematic uncertainties. The uncertainty for the CC and CP channels are $< 0.1\%$ so are ignored. For the CC (CP) conversion channel the maximum uncertainty from the test masses is 0.2% (0.4%), which is applied as the systematic error.

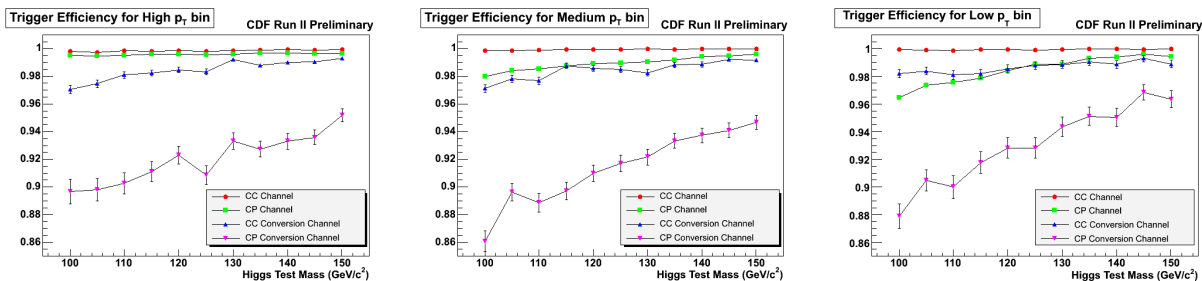


FIG. 1: Trigger efficiencies for each mass and channel in each p_T bin are shown with statistical binomial errors.

IV. PHOTON IDENTIFICATION

A. Central Photon ID

A new method of selecting photons with $|\eta| < 1.05$ was recently developed that takes advantage of a neural network in order to better distinguish true prompt photons from jet backgrounds such as π^0 and η mesons. Since the electron signature is similar to that of photons except for a track, electrons are rejected using the standard set of track cuts that

have been used in the past. This also allows for the possibility of calculating a data-MC scale factor from $Z \rightarrow e^+e^-$ events, where the track cuts are modified to allow a single track.

The selection is given in three steps: (a) loose photon cuts are first applied in order to let the neural net be responsible for harder cases where a jet looks more closely like a photon, (b) standard tight tracking cuts are applied in order to reject electrons and some jets and lastly (c) a cut on the neural network output is applied. Loose cuts require the photons to be in the well instrumented region of the shower maximum detector (fiduciality) and allows for relaxed selection on isolation and the fraction of hadronic E_T . Tighter selection rejects events with significant clusters nearby and events with one or more tracks associated with the electromagnetic cluster that have significant transverse momentum. Finally, a cut on the NN output is applied, optimized for the $H \rightarrow \gamma\gamma$ analysis.

For the CC channel as an example, this selection provides a signal efficiency of 95.5% and background rejection of 81.3%, an improvement from standard cuts which gave 91.6% signal efficiency and 70.6% background rejection.

Efficiencies were calculated using $Z \rightarrow e^+e^-$ decays in both data and MC, as a function of the number of vertices in the event. Net efficiencies were obtained by folding the resulting values into the distribution of the number of vertices in the event for the diphoton data and Higgs MC simulation. A correction factor of 94.7% is derived for the ID efficiency of the simulation by comparing the ID efficiency from the detector simulation with that measured in the data.

Several sources of systematic uncertainty were considered. Photon ID efficiencies are studied using electrons from Z boson decays, however, there are small differences in the shower profiles of electrons and photons which may affect these studies. To account for this, a systematic of 1% was taken based on the difference between photon and electron ID efficiencies observed in the MC with detector simulation. For this comparison, $\gamma \rightarrow e^+e^-$ conversions were removed from the photon MC which are not in the Z MC. An uncertainty of 0.2% on the efficiency of removing these conversions is applied and is due to the uncertainty on material included in the simulation of the CDF detector. A single data-MC scale factor is applied to the full MC sample, however, the variations of this factor between data taking periods was included as a systematic of 1.5%. Finally, the uncertainties on the fits used to study ID efficiencies are propagated as an uncertainty of 0.2%.

B. Plug Photon ID

We include photons with $1.2 < |\eta| < 2.8$ using standard CDF photon ID including fiduciality, isolation, an insignificant fraction of hadronic E_T , and and transverse shower profiles consistent with a single photon. Scale factors are obtained using the same techniques as for central photons, resulting in a simulation correction factor of 90.7%. The same sources of systematic uncertainty on photon ID for central photons are applied to plug photons. Uncertainty from the difference between electron vs photon ID is taken to be 2.6%, from detector material to be 3.0%, from data taking periods to be 2.0%, and from data/MC fits to be 0.8%.

C. Central Conversion Photon ID

As photons pass through detector material, electromagnetic interactions with a nucleus can cause photons to convert into an electron-positron pair. Using photon MC truth information it was found that this occurs approximately 15% of the time in the central region of the detector, so for the CC channel about 26% of events are lost (where we ignore double conversion events) and about 15% of events are lost in the CP channel. Due to lower tracking efficiency in the plug region we only consider central conversion photons.

For the CC and CP conversion channels, events are first considered if a single regular photon is found either in the central or plug region using the identification described in previous sections (thus also rejecting events with a regular CC or CP diphoton pair). A base set of selection is then applied that searches for a primary central electron with a colinear, oppositely signed track nearby. The proximity of the two electron tracks is determined from their $r - \phi$ separation and $\Delta\cot\theta$, or separation in $\cot\theta = p_z/p_T$. “Trident” $e + (\gamma \rightarrow e^+e^-)$ events are rejected by finding cases where there are two tracks near the primary electron that pass this base selection — these are events where an electron radiates a photon via bremsstrahlung which then converts to an electron-positron pair.

A tighter set of selection is then applied to this base criteria. The tracks from both electrons are to point to a fiducial electromagnetic energy cluster (or clusters if in different calorimeter towers). Photons of a higher p_T range are selected by requiring the secondary electron to have a $p_T > 1.0$ GeV/c and the reconstructed conversion photon have $p_T > 15$ GeV/c. In order to reject jet backgrounds, only a small fraction of hadronic E_T associated with the primary electron’s cluster is allowed. Additionally, requirements are made on the conversion candidate’s calorimeter isolation which is obtained from the primary electron’s isolation energy with the secondary electron’s p_T subtracted if it’s track points to a different calorimeter phi tower. The shape describing the ratio of transverse energy to transverse

momentum (E/P) is peaked at one for isolated photon conversions, but has a long tail for photon conversions from π^0 or $\eta \rightarrow \gamma\gamma$ decays due to the extra energy from the unconverted photon. Restrictions on this ratio then provide a further way to remove jet backgrounds. The conversion E_T is obtained from the primary electron's E_T with the secondary electron's p_T added if it is in a different calorimeter tower while the photon's reconstructed transverse momentum is obtained by adding the vector sum of the two tracks momenta at the radius of the conversion. A final requirement removes events with a small radius of conversion, primarily to reduce prompt electron-positron pairs from Dalitz decays of neutral pions $\pi^0 \rightarrow e^+e^-\gamma$.

In order to obtain an uncertainty on identifying the pair conversions, Z decays in both data and MC were again studied as with regular photons. However, after tagging one tight electron, rather than searching for another isolated electron a trident event was studied in order to probe the conversion from the radiated photon. Due to the lower energy range of the conversion photons of this method compared to those from $H \rightarrow \gamma\gamma$, it was chosen not to apply a data-MC scale factor to simulated events but instead to use the difference in the calculated scale factor from one to obtain an uncertainty on conversion ID. This was estimated by comparing the ratio of number of trident events selected to the number of regular $Z \rightarrow e^+e^-$ events selected in both the data and MC. This ratio was chosen in order to remove dependence on uncertainties from sources such as trigger efficiency, luminosity, and Z cross section. The result gives a 7% uncertainty which is applied as a systematic on conversion ID.

V. DETECTOR ACCEPTANCE

The detector acceptance was studied using PYTHIA Monte Carlo production events passed through a simulation for the CDF detector, CDFSIM, based on GEANT [18] and GFLASH [19]. The remaining events that additionally passed the same photon ID selection as the data, were then used to obtain an overall signal acceptance for each signal process and mass point. The acceptance values are given in the following Tables II, III, and IV.

Production Process	M_H (GeV/ c^2)	Signal Acceptances (%)			
		CC	CP	CC Conv	CP Conv
VH	100	5.01	4.10	1.02	.37
	105	5.27	4.33	1.05	.44
	110	5.57	4.65	1.14	.47
	115	5.80	5.13	1.16	.48
	120	5.96	5.43	1.26	.54
	125	6.24	5.73	1.29	.57
	130	6.47	5.97	1.31	.56
	135	6.60	6.29	1.36	.63
	140	6.97	6.62	1.40	.63
	145	7.06	6.84	1.46	.66
	150	7.27	7.02	1.45	.68
VBF	100	4.88	3.82	1.02	.38
	105	4.99	3.98	1.04	.41
	110	5.04	4.29	1.07	.43
	115	5.15	4.37	1.10	.43
	120	5.17	4.63	1.07	.45
	125	5.23	4.71	1.10	.46
	130	5.34	4.88	1.11	.48
	135	5.36	4.99	1.14	.51
	140	5.46	5.05	1.14	.51
	145	5.50	5.17	1.10	.51
	150	5.63	5.24	1.21	.53

TABLE II: Signal acceptance for each signal process, mass point, and channel for the high p_T bin.

VI. SYSTEMATIC UNCERTAINTIES ON SIGNAL

Systematic uncertainties on signal MC are summarized in Table V and include uncertainties in the production cross section, the integrated luminosity, and on the acceptance and efficiency. A 6% uncertainty on the integrated luminosity considers uncertainty in $p\bar{p}$ inelastic cross section and acceptance of CDF's luminosity monitor. The

Production Process	M_H (GeV/ c^2)	Signal Acceptances (%)			
		CC	CP	CC Conv	CP Conv
VH	100	4.90	6.41	1.10	.69
	105	4.80	6.51	1.10	.72
	110	4.80	6.49	1.08	.70
	115	4.78	6.38	1.07	.70
	120	4.73	6.39	1.10	.69
	125	4.66	6.23	1.06	.72
	130	4.64	6.19	1.06	.70
	135	4.56	6.04	1.02	.66
	140	4.52	5.94	1.02	.64
	145	4.47	5.88	.97	.64
	150	4.45	5.79	.97	.65
VBF	100	5.65	6.55	1.27	.70
	105	5.64	6.69	1.31	.77
	110	5.73	6.66	1.33	.74
	115	5.78	6.73	1.33	.78
	120	5.76	6.74	1.33	.75
	125	5.81	6.83	1.32	.73
	130	5.87	6.75	1.39	.79
	135	5.87	6.76	1.32	.76
	140	5.92	6.80	1.33	.74
	145	5.88	6.63	1.36	.76
	150	5.95	6.58	1.34	.74

TABLE III: Signal acceptance for each signal process, mass point, and channel for the medium p_T bin .

Production Process	M_H (GeV/ c^2)	Signal Acceptances (%)			
		CC	CP	CC Conv	CP Conv
VH	100	2.81	3.96	.63	.43
	105	2.67	3.75	.64	.45
	110	2.60	3.70	.59	.41
	115	2.51	3.53	.55	.39
	120	2.40	3.35	.53	.38
	125	2.34	3.20	.53	.38
	130	2.24	3.10	.51	.35
	135	2.22	3.01	.48	.34
	140	2.10	2.82	.49	.33
	145	2.06	2.73	.47	.32
	150	1.97	2.67	.45	.30
VBF	100	3.25	4.18	.77	.50
	105	3.25	4.18	.77	.50
	110	3.28	4.15	.76	.50
	115	3.28	4.14	.73	.47
	120	3.25	4.08	.76	.46
	125	3.19	4.01	.73	.46
	130	3.22	4.00	.76	.46
	135	3.23	3.89	.74	.44
	140	3.26	3.87	.73	.46
	145	3.26	3.82	.72	.45
	150	3.26	3.83	.72	.42

TABLE IV: Signal acceptance for each signal process, mass point, and channel for the low p_T bin.

theoretical uncertainties on the production cross sections used are 7% for associative Higgs production with a W or Z , and 5% for vector boson fusion. All systematics on ID efficiency for photons were described in section IV.

The PDF uncertainty on event acceptance was calculated using the CTEQ61.M [20, 21] error sets and a standard event re-weighting technique [22, 23]. Initial and final state radiation (ISR and FSR) uncertainties were studied using MC samples with modified parton shower parameters and we correlate them. The energy scale systematic uncertainty of the central/plug electromagnetic calorimeters (CEM/PEM) was studied by checking the effect on the acceptance of varying the CEM/PEM scale by 1% to obtain 0.1% for central and 0.8% for plug.

The vertex systematic takes into account the efficiency of reconstructing vertices in an event. Since events are required to lie in the region of the detector consistent with $p\bar{p}$ interactions, the vertex systematic additionally takes into account the fraction of collisions that do not.

The uncertainty on PYTHIA modeling of the shape of the $p_T^{\gamma\gamma}$ distribution for the signal was estimated to be (4%) for the high p_T bin and (2%) for the medium and low p_T bins. The latter uncertainty was estimated by studying the effect on the acceptance from the differences in the shape of the p_T distribution from leading-order, next-to-leading order, Collins-Soper-Sterman (CSS) and PYTHIA predictions [24].

	CDF Run II Preliminary $\int \mathcal{L} = 7.0 \text{ fb}^{-1}$			
	Systematic Errors on Signal (%)			
	CC	CP	CC Conv	CP Conv
Luminosity	6	6	6	6
σ_{VH}	7	7	7	7
σ_{VBF}	5	5	5	5
PDF	2	2	2	2
ISR/FSR	6	8	4	10
Energy Scale	0.2	0.8	0.1	0.8
Trigger Efficiency	–	–	0.1	0.4
Z Vertex	0.2	0.2	0.2	0.2
Conversion ID	–	–	7	7
Material Uncertainty	0.4	3.0	0.2	3.0
Photon/Electron ID	1.0	2.8	1.0	2.6
Run Dependence	3.0	2.5	1.5	2.0
Data/MC fits	0.4	0.8	1.5	2.0
$p_T^{\gamma\gamma}$ PYTHIA/NLO	4	4	4	4

TABLE V: Summary of systematic errors applied to signal.

VII. BACKGROUND MODEL

We are searching for a very narrow peak which is limited only by detector resolution on a smooth background distribution. For regular photons, this smooth region of the data is composed of both SM diphoton events and events in which one or two jets fake a photon. For conversion photons, this region of the data is mostly composed of real conversions from jets and jets faking a conversion photon. Modeling of the background combinations is possible, but non-trivial, and is not necessary for dedicated searches for a narrow mass peak. Therefore, rather than model each background component directly, a null hypothesis is assumed after visual confirmation that no significant peak exists in the data, a smooth curve is fit to the data. This fit excludes a 12 GeV/ c^2 window around each mass point and is then interpolated into the signal region. The fit in the 12 GeV/ c^2 signal region serves as the background model for predicting the expected sensitivity and for testing against the data for the signal hypotheses at the various mass points.

In this analysis, we considered three p_T bins. For the high and medium p_T bins, the statistics were low and we used a fitting function with only four parameters. Moreover, we fit using sidebands on the high mass end up to 220 GeV for the regular photon channels, but the conversion channels run out of events in this range, so we only fit up to 180 GeV.

For the lower p_T bin, the statistics were high and we used a function with six parameter. One modification to this method is made for the CP channels that are contaminated by a large contribution of $Z \rightarrow e^+e^-$ backgrounds which is visible as a peak in the data. The Z background could be modeled by MC and added then to the smooth portion, but we can also more simply further our current method by adding an appropriate function to describe the peak made by the Z boson. It was found that a Breit-Wigner function well describes this region of the $M_{\gamma\gamma}$ distribution for the CP channels, so it was added to the smooth function used to fit to the rest of the data.

An example fit for each channel, obtained from a mass window around 120 GeV/ c^2 , is shown in Figures 2 – 3, along with the corresponding residual plot of $(\text{data} - \text{fit})/(\text{stat error})$. The stability of the fits in the 12 GeV/ c^2 signal region used for setting limits was studied by fluctuating the parameter values of the fit and then taking the average of the smallest and largest integral differences from that of the standard function. In general, these values reflect the statistics in the respective mass distributions as higher statistics constrains the amount by which the fit will fluctuate as parameter values are varied. The results were used to obtain a background rate uncertainties for each channel and

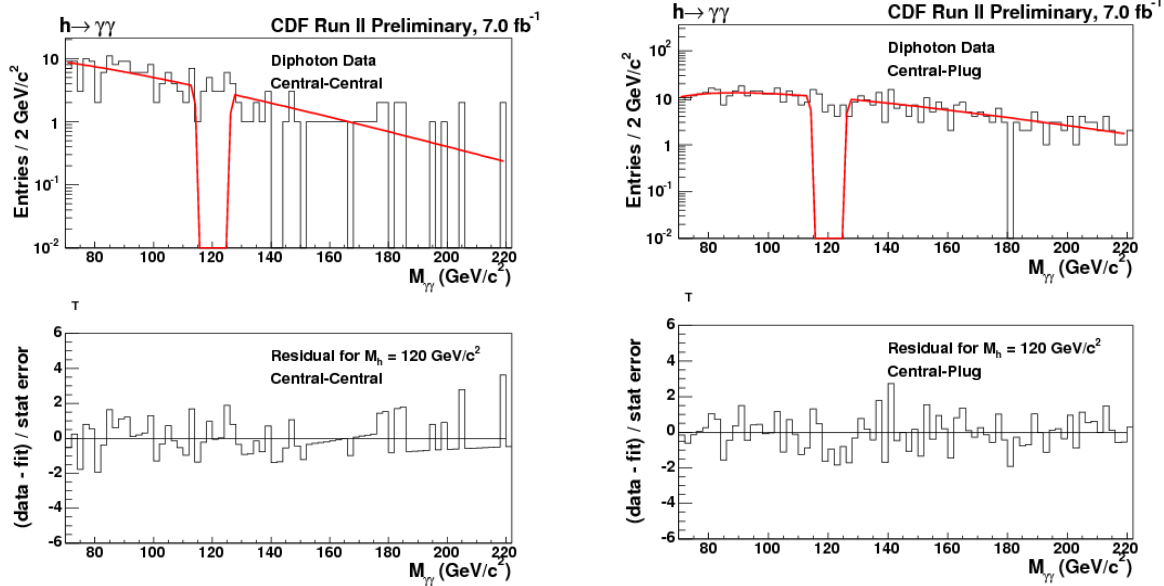


FIG. 2: Smooth fits to the signal region in the data for CC channel (left) and CP channel (right) with the fermiophobic Higgs event selection for the high p_T bin. The example fit shown was obtained by first excluding a $12 \text{ GeV}/c^2$ window around a signal mass of $M_h = 120 \text{ GeV}/c^2$ and then interpolating into this region. The fit in the signal region will serve as the null hypothesis background model. The data-fit residuals are also shown.

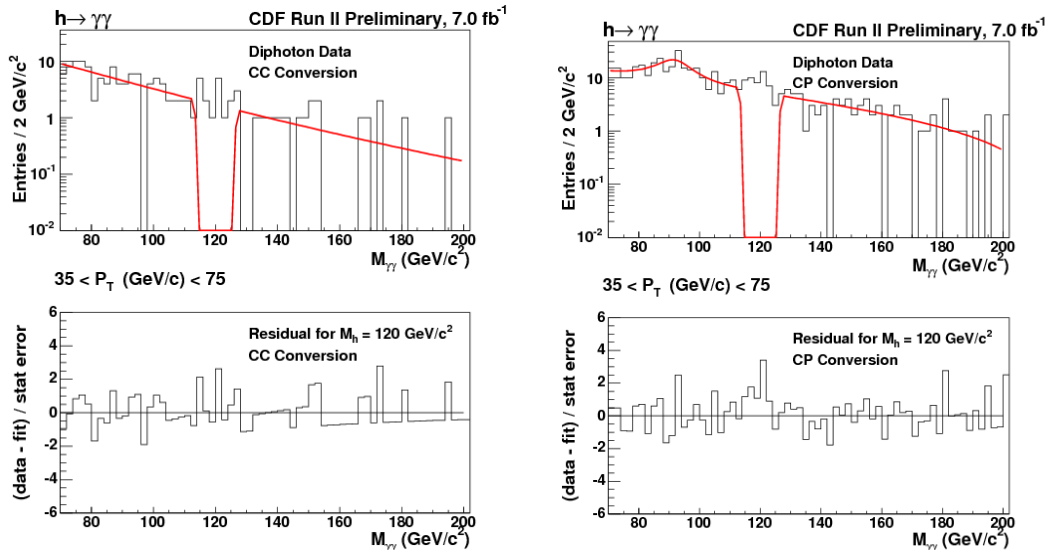


FIG. 3: Smooth fits to the signal region in the data for CC conversion channel (left) and CP conversion channel (right) with the fermiophobic Higgs event selection for the medium p_T bin. The example fit shown was obtained by first excluding a $12 \text{ GeV}/c^2$ window around a signal mass of $M_h = 120 \text{ GeV}/c^2$ and then interpolating into this region. The fit in the signal region will serve as the null hypothesis background model. The data-fit residuals are also shown.

mass are about 11.4%, 6.1%, 28.1%, and 25.2% applied to the CC, CP, CC conversion, and CP conversion channels respectively in the case of high p_T bin. For the medium p_T bin, we found that the background rate uncertainties for each channel and mass are about 8.1%, 2.6%, 15.2%, and 13.6% applied to the CC, CP, CC conversion, and CP conversion channels respectively. Finally, we found that the background rate uncertainties for each channel and mass are about 3.9%, 1.1%, 8.6%, and 3.7% applied to the CC, CP, CC conversion, and CP conversion channels respectively for the low p_T bin. Cross checks on these values were done by either replacing or modifying the fit function. From these studies, variations of the test background yields in the signal regions as compared to that of the standard were consistent with uncertainties already obtained.

VIII. RESULTS

We set upper limits on production cross sections times branching ratio and the branching ratio for a Fermiophobic Higgs. We calculate a Bayesian C.L. limit for each mass hypothesis based on the combined binned likelihood of the mass distributions for each channel. The results of the limit calculation are included in Table VI and displayed graphically in Figure 4. The SM cross sections in the benchmark fermiophobic model are used to convert the limits on $\sigma \times Br(h \rightarrow \gamma\gamma)$ into limits on $Br(h \rightarrow \gamma\gamma)$. The result sets an observed (expected) limit on the Fermiophobic Higgs boson production excluding Higgs bosons particles with a mass $m_{h,f} > 114$ GeV/c² ($m_{h,f} > 111$ GeV/c²) at the 95% confidence level.

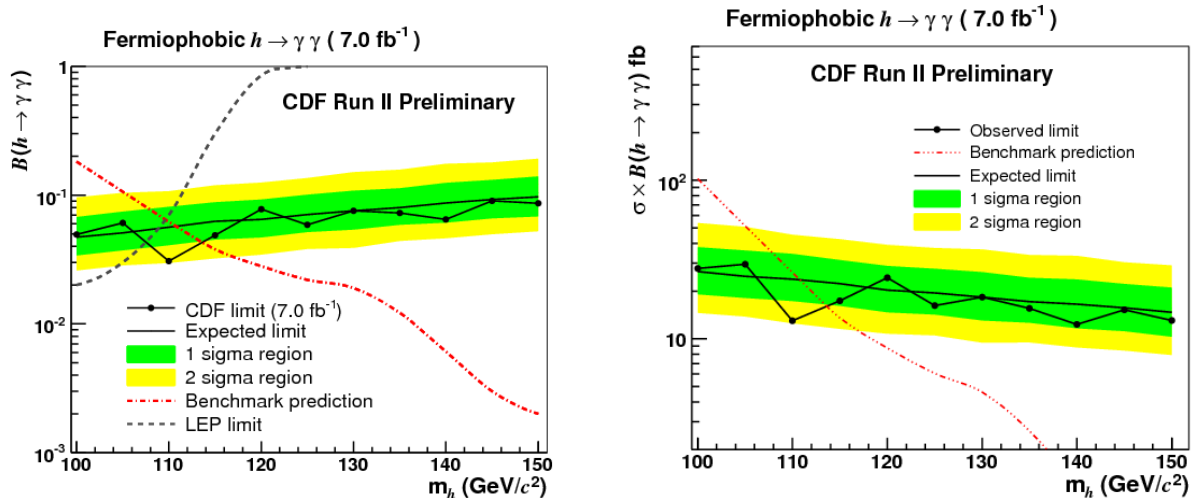


FIG. 4: The 95% C.L. upper limit on the branching fraction for the fermiophobic Higgs boson decay to diphotons, as a function of m_h (left). Similarly for the branching ratio times cross section (right).

CDF Run II Preliminary				$\int \mathcal{L} = 7.0 \text{ fb}^{-1}$		
m_h (GeV/c ²)	$\sigma \times Br(h \rightarrow \gamma\gamma)$ Limits (fb)			$Br(h \rightarrow \gamma\gamma)$ Limits (%)		
	Expected	Observed	Model expectation	Expected	Observed	Model expectation
100	26.5	27.7	102.2	4.7	4.9	18.2
105	24.7	29.5	51.5	5.0	6.0	10.6
110	23.7	13.0	26.2	5.6	3.0	6.2
115	22.3	17.3	13.5	6.2	4.8	3.8
120	20.2	24.3	8.7	6.4	7.7	2.8
125	19.4	16.1	6.0	7.0	5.8	2.2
130	18.3	18.3	4.6	7.5	7.5	1.9
135	17.1	15.5	2.6	7.9	7.2	1.22
140	16.5	12.3	1.1	8.6	6.4	0.61
145	15.6	15.2	0.5	9.2	9.0	0.3
150	14.6	13.0	0.3	9.7	8.6	0.2

TABLE VI: Observed and expected 95% C.L. limits on the production cross section and branching fraction and theory predictions for the fermiophobic benchmark Higgs boson model.

IX. CONCLUSIONS

We presented the results of a search for a narrow resonance in the diphoton mass spectrum using data taken by the CDF II detector at the Tevatron 7.0 fb⁻¹. There is no evidence of a narrow resonance. Limits are placed on the production cross section and the branching fraction for the Higgs boson decay into a photon pair and compared to the predictions of a benchmark fermiophobic model. We found an observed (expected) limit on the Fermiophobic Higgs

boson production excluding Higgs bosons particles with a mass $m_{hf} < 114 \text{ GeV}/c^2$ ($m_{hf} < 111 \text{ GeV}/c^2$) at the 95% confidence level.

Acknowledgments

We thank the Fermilab staff and the technical staffs of the participating institutions for their vital contributions. This work was supported by the U.S. Department of Energy and National Science Foundation; the Italian Istituto Nazionale di Fisica Nucleare; the Ministry of Education, Culture, Sports, Science and Technology of Japan; the Natural Sciences and Engineering Research Council of Canada; the National Science Council of the Republic of China; the Swiss National Science Foundation; the A.P. Sloan Foundation; the Bundesministerium fuer Bildung und Forschung, Germany; the Korean Science and Engineering Foundation and the Korean Research Foundation; the Particle Physics and Astronomy Research Council and the Royal Society, UK; the Russian Foundation for Basic Research; the Comision Interministerial de Ciencia y Tecnologia, Spain; and in part by the European Community's Human Potential Programme under contract HPRN-CT-20002, and the Academy of Finland.

-
- [1] A. Barroso, L. Brucher, and R. Santos, Phys. Rev. **D60**, 035005 (1999), hep-ph/9901293.
 - [2] J. Gunion, R. Vega, and J. Wudka, Phys. Rev. **D42**, 1673 (1990).
 - [3] S. Mrenna and J. D. Wells, Phys. Rev. **D63**, 015006 (2001), hep-ph/0001226.
 - [4] G. L. Landsberg and K. T. Matchev, Phys. Rev. **D62**, 035004 (2000), hep-ex/0001007.
 - [5] L. Authors (LEP Higgs Working Group) (2001), hep-ex/0107035.
 - [6] A. A. Affolder et al. (CDF), Phys. Rev. **D64**, 092002 (2001), hep-ex/0105066.
 - [7] V. Abazov et al. (D0) (2008), arXiv:0803.1514 [hep-ex].
 - [8] T. Aaltonen et al. (CDF), Phys. Rev. Lett. **103**, 061803 (2009), 0905.0413.
 - [9] V. Abazov et al. (D0), Phys. Rev. Lett. **102**, 231801 (2009).
 - [10] M. Spira (1998), hep-ph/9810289.
 - [11] F. Abe et al. (CDF), Nucl. Instr. Meth. **A271**, 387 (1988).
 - [12] P. T. Lukens (CDF IIb) (2003), FERMILAB-TM-2198.
 - [13] T. Sjostrand et al., Comput. Phys. Commun. **135**, 238 (2001), hep-ph/0010017.
 - [14] H. L. Lai et al. (CTEQ), Eur. Phys. J. **C12**, 375 (2000), hep-ph/9903282.
 - [15] R. Field and R. C. Group (CDF) (2005), hep-ph/0510198.
 - [16] T. Aaltonen et al. (CDF) (2007), arXiv:0707.2294 [hep-ex].
 - [17] C. collaboration (CDF) (2010), CDF note 10065.
 - [18] R. Brun, F. Bruyant, M. Maire, A. C. McPherson, and P. Zancarini (1987), CERN-DD/EE/84-1.
 - [19] G. Grindhammer, M. Rudowicz, and S. Peters, Nucl. Instrum. Meth. **A290**, 469 (1990).
 - [20] D. Stump et al., JHEP **10**, 046 (2003), hep-ph/0303013.
 - [21] J. Pumplin et al., Phys. Rev. **D65**, 014013 (2002), hep-ph/0101032.
 - [22] P. M. Nadolsky and Z. Sullivan, eConf **C010630**, P510 (2001), hep-ph/0110378.
 - [23] D. Bourilkov, R. C. Group, and M. R. Whalley (2006), hep-ph/0605240.
 - [24] S. Mrenna and C. P. Yuan, Phys. Lett. **B416**, 200 (1998), hep-ph/9703224.